Coaxial Omnidirectional Stereopsis

Libor Spacek

Department of Computer Science
University of Essex
Colchester, CO4 3SQ, UK
spacl@essex.ac.uk,
http://cswww.essex.ac.uk/mv

Abstract. Catadioptric omnidirectional sensors, consisting of a camera and a mirror, can track objects even when their bearings change suddenly, usually due to the observer making a significant turn. There has been much debate concerning the relative merits of several possible shapes of mirrors to be used by such sensors.
This paper suggests that the conical mirror has some advantages over other shapes of mirrors. In particular, the projection beam from the central region of the image is reflected and distributed towards the horizon rather than back at the camera. Therefore a significant portion of the image resolution is not wasted.
A perspective projection unwarping of the conical mirror images is developed and demonstrated. This has hitherto been considered possible only with mirrors that possess single viewpoint geometry. The cone is viewed by a camera placed some distance away from the tip. Such arrangement does not have single viewpoint geometry. However, its multiple viewpoints are shown to be dimensionally separable.
Once stereopsis has been solved, it is possible to project the points of interest to a new image through a (virtual) single viewpoint. Successful reconstruction of a single viewpoint image from a pair of images obtained via multiple viewpoints appears to validate the use of multiple viewpoint projections.
The omnidirectional stereo uses two catadioptric sensors. Each sensor consists of one conical mirror and one perspective camera. The sensors are in a coaxial arrangement along the vertical axis, facing up or down. This stereoscopic arrangement leads to very simple matching since the epipolar lines are the radial lines of identical orientations in both omnidirectional images.
The stereopsis results on artificially generated scenes with known ground truth show that the error in computed distance is proportional to the distance of the object (as usual), plus the distance of the camera from the mirror. The error is also inversely proportional to the image radius coordinate, ie. the results are more accurate for points imaged nearer the rim of the circular mirror.

T. Pajdla and J. Matas (Eds.): ECCV 2004, LNCS 3024, pp. 354–365, 2004.
© Springer-Verlag Berlin Heidelberg 2004

1 Introduction

Autonomous navigation, site modelling and surveillance applications all benefit from using panoramic 360° images. Omnidirectional visual sensors produce such images. Early attempts at using omnidirectional sensors included camera clusters [1] and various arrangements of mechanically rotating cameras and planar mirrors, [2], [3], [4]. These mostly had problems with registration, motion, or both. Fisheye lens cameras have also been used to increase the field of view [5] but they proved difficult because of their irreversible distortion of nearby objects and the lack of a single viewpoint, explained below.

Catadioptric sensors [6] consist of a fixed dioptric camera, usually mounted vertically, plus a fixed rotationally symmetrical mirror above or below the camera. The advantages of catadioptric sensors derive from the fact that, unlike the rotating cameras, their 'scanning' of the surroundings is moreless instantaneous. (The camera exposure time is usually shorter than the full rotation time). Shorter exposure means fewer image capture problems caused by motion and vibration of the camera, or by moving objects.

The suitability for use in dynamic environments is clearly an important consideration, especially as one of the chief benefits of omnidirectional vision in general is the ability to retain objects in view even when their bearings have changed significantly. Catadioptric omnidirectional sensors are ideally suited to visual navigation [7], visual guidance applications [8], using stereopsis, motion analysis [9], and site mapping [10].

The problem with catadioptric sensors is that the details of the image can have relatively poor resolution, as the image depicts a large area. The resolution problem is unfortunately compounded by mirrors whose shapes have curved cross-sections. Such radially curved mirrors include the three quadric surface mirrors (elliptic, hyperbolic and parabolic) which are known to possess a single viewpoint at their focal points.

Single viewpoint projection geometry exists when the light rays arriving from all directions intersect at a single point known as the (single) effective viewpoint. For example, by placing the centre of the perspective camera lens at the outer focus of the hyperbolic mirror, the inner focus then becomes the single effective viewpoint.

A single viewpoint is generally thought to be necessary for an accurate unwarping of images and for an accurate perspective projection which is relied on by most computer vision methods [11].

The single viewpoint projection has been endorsed and recommended by [12], [13], [14], [15], [16] and others.

There have been few attempts at analysing non-single viewpoint sensors [17], [18], although various people [19] used them previously without analysis.

The omnidirectional sensors resolution can be improved by using several planar mirrors with a separate camera for each one of them. The mirrors are placed in some spatial arrangement, for instance in a six sided pyramid [20]. The reflected camera positions are carefully aligned to coincide and to form a single effective viewpoint. However, such arrangements are awkward, expensive, and

sensitive to alignment errors. The hexagonal pyramid apparatus would require no fewer than twelve cameras for stereopsis! Also, the coverage of the surrounding area is not isotropic.

Spacek [21] proposed a solution to the above problems which combines the benefits of the planar mirrors (no radial distortion, no radial loss of resolution) with the advantages of the rotationally symmetric catadioptric sensor (short exposure, isotropic imaging). The only shape of mirror that satisfies these requirements is the cone.

2 Perspective Projection through a Conical Mirror

The benefits of the cone mirror over the radially curved mirrors were pointed out by Lin and Bajczy in [22]. They can be summarised as:
1. Curved cross-section mirrors produce inevitable radial distortions. Radial distortion is proportional to the radial curvature of the mirror. The cone has zero radial curvature everywhere except at its tip, which is only reflecting the camera anyway.
2. Radially curved mirrors produce 'fish eye' effects: they magnify the objects reflected in the centre of the mirror, typically the camera, the robot, or the sky, all of which are of minimal interest. On the other hand, they shrink the region around the horizon, thereby reducing the available spatial resolution in the area which is of interest. See Figures 1 and 2 for the comparison of the hyperbolic and the conical mirrors. The mirrors are showing different scenes but both are pointing vertically upwards.
3. The cone presents planar mirrors in cross-section. See Figure 3. The planar mirror does not have a complicated function mapping the camera resolution density onto the real world.

Some optimised shapes of radially curved mirrors have been proposed [23], as well as hybrid sensors, mirrors combining two shapes into one, and other mirrors of various functions. However, it seems that none of them completely address all of the above points.

The cone mirror has a single effective viewpoint located at the tip. Lin and Bajczy proposed cutting off the tip and placing the camera lens in its place, or placing the tip at the forward focus point of the lens. Both of these methods require the camera to be very close to the mirror which results in difficulties with capturing enough light and with focusing, so the improvement in image quality over the curved mirrors is debatable.

Our solution consists of placing the camera at a comfortable distance d from the tip of the conical mirror and still obtaining a useful projection, despite the fact that there is now an infinite number of viewpoints arranged in a circle of radius d around the tip of the cone. See Figure 4. Not having to fix the camera at a precise distance represents an additional practical benefit in comparison with the hyperbolic mirrors or the approach of Lin and Bajczy.

R is both the radius and the height of the cone with a 90° angle at the tip. Given the field of view angle ϕ of a particular camera lens, the appropriate

Fig. 1. An omnidirectional image obtained using a hyperbolic mirror and an ordinary perspective camera. Note the typical predominance of the sky.

Fig. 2. A conical mirror image of an indoors scene. The entire mirror image reflects useful data.

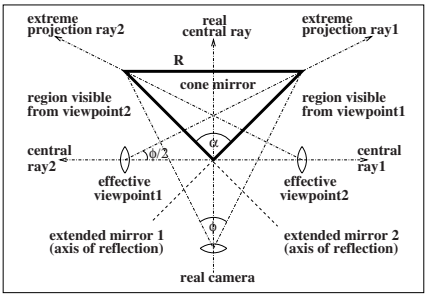

Fig. 3. Cross section of the conical mirror projection geometry. According to the laws of optics, mirrors can reflect either the objects or the viewpoints. The two situations are equivalent. In this case, the real camera with a field of view ϕ is reflected in two planar mirrors, creating two effective viewpoints. Each viewpoint has a field of view $\phi/2$ between its central projection ray and its extreme ray. The angle at the tip of the cone is $\alpha = 90°$ to ensure that the two effective lines of sight (central rays 1&2) are oriented directly towards each other. R is the radius of the mirror.

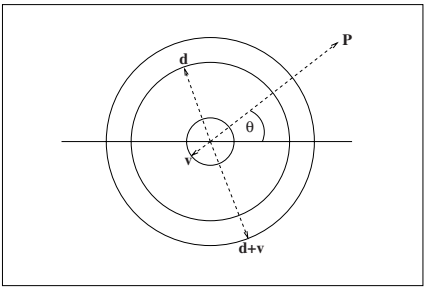

Fig. 4. Top view of the perspective projection of P via the conical mirror. The circle of radius d is the locus of the viewpoints of the distant camera.

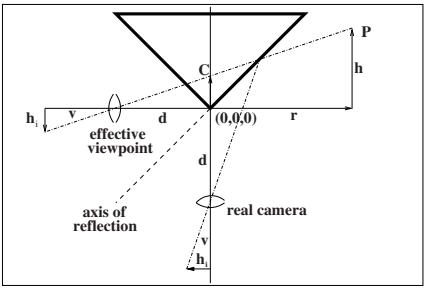

Fig. 5. Cross section of the perspective projection of P via the conical mirror: the image is distance v behind the centre of the lens.

camera distance $d = R(cotan\frac{\phi}{2} - 1)$. This is the camera distance calculated to inscribe the base circle of the cone within the image. The field of view of the camera and the size of the mirror are thus utilised to their best advantage. For example, a mirror of radius $R = 60mm$ and a camera with $\phi = \pi/4$ results in $d = 85mm$ (rounded up). d is critical for the focal mirrors but not so for the cone. At worst, we may lose a few pixels around the edges of the image.

2.1 The Projections

The image of a rotationally symmetric mirror viewed along its axis of symmetry is circular. It is therefore convenient to use the polar coordinates (r_i, θ) to represent the image positions and the related cylindrical coordinates (r, θ, h) for the 3D scene. See Figure 5 for the θ cross section of the conical mirror and the associated perspective projection. Note that the points of interest along the projection ray from a 3D scene point $P(r, \theta, h)$ are collinear (forming three similar triangles).

Let the image radius coordinate r_i of the projected point P have the value h_i (the image height of P). The perspective projection formula is obtained from the collinearity property (or two similar triangles) in Figure (5):

$$h_i = \frac{vh}{d + r} \tag{1}$$

h_i values are always positive (image radius). This is equivalent to using front projection to remove the image reversal. Equation (1) is much simpler than the projection equations for the radially curved mirrors.

v is the distance of the image plane behind the centre of the thin lens in Gaussian optics. The focal length is normally less than v, unless we reduce v to focus on infinity, or use the simplifying pinhole camera assumption. The calibration of v is obtained by substituting the image radius of the mirror r_m for h_i, and R for h and r in equation (1), giving: $v = r_m(\frac{d}{R} + 1)$. The image radius r_m is determined by locating the outer contour of the mirror in the image.

The classic perspective projection function for the single effective viewpoint at $(0, 0, 0)$ is just a special case of equation (1), where $d = 0$. Suppose we create a thought-experiment (Gedanken) world in which all the objects are pushed distance d further away from the mirror axis. Then the single viewpoint projection of the Gedanken world would result in the same image as the multiple viewpoint projection of the real world. It is also clear that once r is known (see the stereopsis method below), it is possible to reconstruct the single viewpoint projection of the real world by using equation (1) and setting $d = 0$.

The geometry is illustrated in Figure 4. The outer circle depicts the projection cylinder with the radius $d + v$ and the same axis as the cone. The projection cylinder for the single viewpoint at $(0, 0, 0)$ is similar but has the radius v (the innermost circle).

So far, we considered the projection for a fixed value of θ and identified its associated viewpoint. Now we fix the elevation angle $\epsilon = \arctan(h/(d + r))$ and allow θ to vary. Imagine spinning Figure 5 around the mirror axis. All projection

lines with the same elevation angle will intersect the cone axis at the single point $C(0, \theta, h_c)$. Thus the intersection point C is the viewpoint associated with the elevation ϵ. We can determine the height h_c of C from the height h of P by again using the collinearity property: $h_c = (d \cdot h)/(d + r)$.

Sensors with a single (global) effective viewpoint have the same perspective projection in both orthogonal image dimensions (usually x, y). However, we get a different perspective projection in the θ dimension, as the effective viewpoint C for the θ dimension is different from the effective viewpoint $(d, \theta + \pi, 0)$ for the radial projection.

θ projection is not needed for our stereopsis which uses only the radial projection but it could be utilised if we placed two mirrors side-by-side. It has been used in this fashion in [24].

We now define the projection property whereby the viewpoints are said to be dimensionally separable:
– Each radial line in the image (or equivalently each column in the unwarped image) has its own unique viewpoint.
– Each concentric circle in the image (or equivalently each row in the unwarped image) has its own unique viewpoint.
– Each pixel is aligned with its two (row and column) viewpoints, along the projection line from P.

2.2 Registration

We have just described the idealised projection which will be valid and accurate after registration, when the tip of the mirror is precisely aligned with the centre of the image and the axis of view coincides with the axis of the mirror. In general, registration needs to be performed to find the two translation and three rotation parameters needed to guarantee this. Existing registration methods will also apply and work in this situation. See [25] and [26] for good solutions to this problem within the context of omnidirectional vision.

Straight lines in the 3D world become generally conic section curves when projected. However, lines which are coplanar with the axis of the mirror project into radial lines. Concentric circles around the mirror project again into concentric circles. These properties can be utilised for a simple test card registration method, where the test card is of the 'shooting target' type consisting of crosshairs and concentric circles, centered on the cone axis.

2.3 Unwarping of the Input Image

If we were to cut and unroll the virtual projection cylinder, we would get the unwarped rectangular panoramic image. Therefore unwarping is the backprojection of the real input image onto the virtual projection cylinder. The unwarping from the polar coordinates (h_i, θ_i) of the input image into the (x, y) coordinates of the rectangular panoramic image is:

$$x = \frac{x_m}{2\pi} \cdot \theta_i \quad , \quad y = \frac{y_m}{r_m} \cdot h_i \tag{2}$$

where (x_m, y_m) are the desired dimensions of the unwarped image, r_m is the radius of the mirror as seen in the input image, and θ_i is measured in radians. The aspect ratio of the panoramic image is: $x_m/y_m = 2\pi$.

The direct mapping from the pixel position (x, y) of the panoramic unwarped image to the corresponding position (x_i, y_i) of the input image is presented next. We use polar coordinates as an intermediate step, and then equations 2. We also need to know the centre of the mirror in the input image (x_c, y_c).

$$x_i = x_c + h_i \cdot \cos\theta_i = x_c + \frac{r_m}{y_m} \cdot y \cdot cos(\frac{2\pi}{x_m} \cdot x) \tag{3}$$

$$y_i = y_c + h_i \cdot \sin\theta_i = y_c + \frac{r_m}{y_m} \cdot y \cdot sin(\frac{2\pi}{x_m} \cdot x) \tag{4}$$

We used the unwarping by two dimensional DCT (discrete cosine transform) of the omnidirectional input image, as described in [21], instead of the usual but less precise pixel interpolation methods. The main advantage of this approach becomes apparent when performing the radial edge-finding needed for our stereo (see the next section).

See Figure 6 for the unwarping applied to a hyperbolic mirror image and Figure 7 for the unwarping of a conical mirror image. Note that the conical mirror image utilises better the available vertical resolution of the image. This provides better resolution for stereopsis, though the resolution near the tip of the mirror is clearly limited.

Fig. 6. Unwarping of Figure 1.

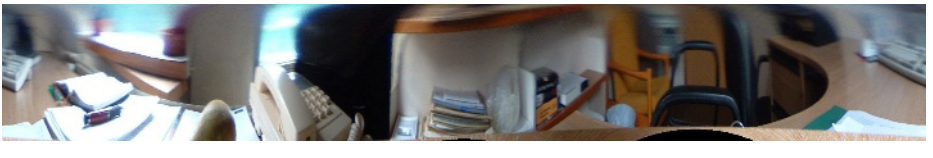

Fig. 7. Unwarping of Figure 2.

3 Coaxial Stereopsis

Various arrangements have been proposed for binocular systems using catadioptric sensors. Two mirrors situated side by side can be used to compute the distance of objects in terms of the disparity measured as the arising difference in angles θ [24]. However, such arrangement is not truly omnidirectional, as a large part of the scene will be obstructed by the other catadioptric sensor.

It is better to arrange the cameras coaxially to avoid this problem. The coaxial arrangement has the further major advantage of having simple aligned radial epipolar lines. Lin and Bajczy [27] used a single conical mirror and attempted to place two cameras at different distances along its axis. They had to use a beam-splitter to avoid the nearer camera obstructing the view of the more distant camera. See Figure 8. We propose an omnidirectional stereo system consisting

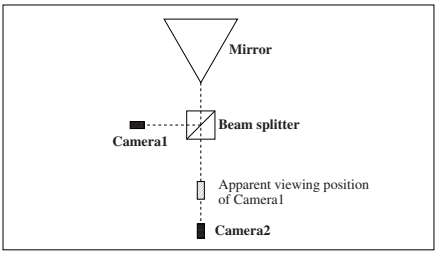

Fig. 8. Lin and Bajcsy's omnidirectional stereo using a single conical mirror and two cameras at different distances. The beam splitter avoids an obstruction of the second camera's view but reduces the amount of available light.

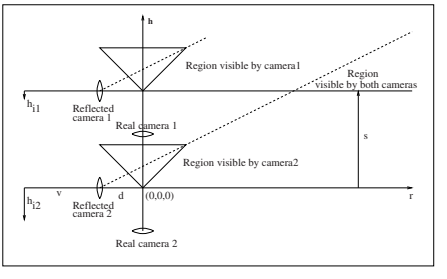

Fig. 9. Omnidirectional stereo using two coaxial mirrors.

of two coaxial conical mirrors pointing in the same direction, each with its own camera. See Figure 9.

We wish to obtain a triangulation formula for the radial distance of objects r. The radial distance is measured from the axis of the mirror(s) to any 3D scene point P, which has to be in the region that is visible by both cameras (the common region). See Figure 9. The common region is annular in shape in 3D, with a triangular cross-section extending to infinity. It is bounded above and below in the (r, h) plane by the lines: $h = R\frac{r+d}{R+d}$, and $h = s$. The angle at the tip of the common region triangle is $\frac{\phi}{2}$. The distance r_{min} of the tip is: $r_{min} = s(\frac{d}{R} + 1) - d$. Stereopsis cannot be employed anywhere nearer than r_{min}.

In order to obtain the triangulation formula, we subtracted two instances of equation (1) for two coaxial mirrors separated by distance s (s is measured along the h axis). We assume here that the parameters v and d are the same for both

cameras, though this assumption can be easily relaxed if necessary.

$$r = \frac{vs}{h_{i2} - h_{i1}} - d \tag{5}$$

This is very similar to the usual triangulation formula from classical side-by-side stereopsis but here the disparity $h_{i2} - h_{i1}$, is the radial disparity. The extra distance d is correctly subtracted.The similarity of the formulae is not surprising, as the two reflected (virtual) cameras resemble a classical side-by-side system within the plane of orientation θ.

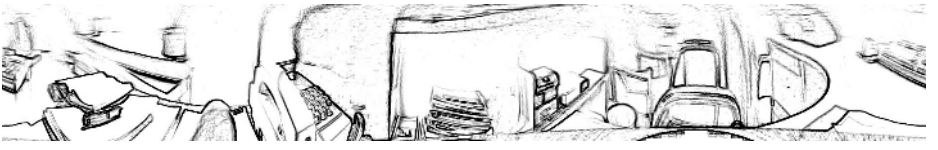

Fig. 10. Edge map of the unwarped image in Figure 7.

3.1 Radial Edge Finding and Matching

The radial epipolar matching is driven by edges whose gradient is primarily in the radial direction. We find those by the radial edge-finder using the DCT and the polar coordinates (h_i, θ_i) of the input image, as described in [21]. The main benefit of this approach is that the slow unwarping process is avoided. We also obtain the partial derivatives of the image function in h_i and θ_i directions, which is going to be useful for a polar optic flow.

The unwarping is needed only for the convenience of human viewing, such as in Figure 10, showing a traditional edge map of the unwarped image, using [28]. The stereopsis correspondence computation is driven primarily by the horizontal edges in this example.

The radial edge finding consists of the following steps:
1. Perform forward DCT transform on the omnidirectional input image, using (x_i, y_i) coordinates.
2. Convert the input image coordinates at which the radial gradient component is to be computed from the rectangular form (x_i, y_i) to the polar form (h_i, θ_i) and substitute to the normal inverse DCT function.
3. Apply the radial edge function (ref) defined in [21]. This function was obtained by partial differentiation of the inverse DCT transform in polar coordinates with respect to h_i.

In other words, we are differentiating the inverse transform function instead of differentiating the image. This is legitimate as the DCT has a finite number of terms. The output is the desired radial edge map in the same format as the original input image, ie. it is the radial edge map of the circular mirror in the rectangular image coordinates (x_i, y_i). Similar process can be followed to find the partial derivatives of an image in θ direction, or higher derivatives.

The radial edge finder should be of interest to omnidirectional vision generally, as it can be used with any rotationally symmetric mirror. The unwarping is unnecessary when using autonomous vision methods that work in polar coordinates.

It is not necessary to generate the entire rectangular edge map of the second image when doing the stereo matching. The ref can be evaluated at any randomly selected points with sub-pixel accuracy. The outline of the radial stereo matching algorithm is as follows:
1. Given a pair of stereo images f_1 and f_2, find all feature points in f_1 where $abs(\frac{\partial f_1(x_i,y_i)}{\partial h_i})$ is significant ($abs()$ is the absolute value function).
2. Find out the θ_i value of the selected feature point.
3. Keeping θ_i fixed, evaluate ref along the epipolar radial line in f_2 and store the image gradient vectors for both epipolar lines in two buffers.
4. Match the buffers looking for similar values of the gradient vectors and paying attention to sensible ordering of the matches plus any other stereopsis matching tricks.
5. Compute the distance of objects for all successful matches, using the matched radial position values h_{i1} and h_{i2} and the triangulation equation (5).
6. Move to the next value of θ_i which has significant image feature(s) and repeat from 2.

There are other sophisticated stereo matching methods that could be adapted to these circumstances, for example [29].

3.2 Steropsis Discussion and Results

In the illustrated arrangement the view is directed at the horizon, which is normally rich in natural visual features of high contrast that are useful for outdoors navigation [7]. For closer visual guidance indoors, the entire apparatus can be simply inverted. The visible regions will lie either above or below the horizontal plane touching the tip of the mirror, respectively. For very close range stereo, we suggest inverting just the top mirror and camera, so that the tips of the mirrors are facing away from each other. In each case the following triangulation and matching will be much the same. The only combination to be avoided for stereopsis is the one with the tips of the mirrors facing each other, as this would result in no common region visible by both cameras.

Our arrangement is quite different from that proposed by Lin and Bajczy. The resulting triangulation formula is different. Our system is simpler, there is no loss of light through the beam splitter, and we gain better image quality by being able to view large size conical mirrors.

Lin and Bajczy did not specify a 90° angle at the tip of their mirror so our perspective projection, as described in section 2, has different specific properties.

We have tested our stereopsis method on artificial images with known ground truth (admittedly not as demanding a test as using real images) and found the errors in r to grow linearly with $r + d$. The errors are a function of the image resolution, so for a fixed r, they are inversely proportional to h. This means that the errors are smaller for points imaged nearer the edge of the mirror, where

the θ resolution is better. There is a good agreement between our results and a theoretical error prediction based on differentiation of the perspective projection formula.

4 Conclusion

This paper has identified the conical mirror as a good solution for catadioptric omnidirectional sensors.

The benefits of conical mirrors had been hitherto mostly overlooked because of the demands for a single viewpoint projection. We conclude that the single viewpoint is not necessary for an accurate perspective projection when using the conical mirror with a 90° angle at the tip. Such conical mirrors provide a useful model of projection when viewed from any reasonable distance by an ordinary perspective camera. Conical mirrors are less sensitive to the precise distance of the camera than are hyperbolic and elliptic mirrors. The ability to view the mirror from a greater distance is desirable since it allows the use of larger mirrors with relatively better optical quality. Given the same physical surface quality (roughness), the optical quality will be proportional to the dimensions of the mirror. The radial distortion properties of conical mirrors are better when compared to other circular mirrors. Last but not least, conical mirrors direct the camera resolution into more useful parts of the surroundings and their resolution density is well behaved.

The unwarping methods and experiments demonstrated the concept of an accurate perspective projection via multiple viewpoints.

The benefits of the coaxial omnidirectional stereo system are both practical (objects do not disappear from view due to vehicle rotation), and theoretical/computational (the epipolar geometry is simpler than in classical stereopsis).

References

1. Swaminathan, R., Nayar, S.K.: Nonmetric calibration of wide-angle lenses and polycameras. IEEE Transactions on Pattern Analysis and Machine Intelligence **22** (2000) 1172–1178
2. Rees, D.: Panoramic television viewing system. US Patent No. 3,505,465 (1970)
3. Kang, S., Szeliski, R.: 3-d scene data recovery using omnidirectional multibaseline stereo. IJCV **25** (1997) 167–183
4. Ishiguro, H., Yamamoto, M., Tsuji, S.: Omni-directional stereo. PAMI **14** (1992) 257–262
5. Shah, S., Aggarwal, J.: Mobile robot navigation and scene modeling using stereo fish-eye lens system. MVA **10** (1997) 159–173
6. Nayar, S.: Catadioptric omnidirectional cameras. In: CVPR97. (1997) 482–488
7. Rushant, K., Spacek, L.: An autonomous vehicle navigation system using panoramic vision techniques. In: International Symposium on Intelligent Robotic Systems, ISIRS98. (1998) 275–282
8. Pajdla, T., Hlavac, V.: Zero phase representation of panoramic images for image vased localization. In: Computer Analysis of Images and Patterns. (1999) 550–557

9. Yagi, Y., Nishii, W., Yamazawa, K., Yachida, M.: Rolling motion estimation for mobile robot by using omnidirectional image sensor hyperomnivision. In: ICPR96. (1996)
10. Yagi, Y., Nishizawa, Y., Yachida, M.: Map-based navigation for a mobile robot with omnidirectional image sensor copis. Trans. Robotics and Automation **11** (1995) 634–648
11. Baker, S., Nayar, S.: A theory of single-viewpoint catadioptric image formation. IJCV **32** (1999) 175–196
12. Baker, S., Nayar, S.: A theory of catadioptric image formation. In: ICCV98. (1998) 35–42
13. Geyer, C., Daniilidis, K.: A unifying theory for central panoramic systems and practical applications. In: ECCV00. (2000)
14. Geyer, C., Daniilidis, K.: Properties of the catadioptric fundamental matrix. In: ECCV02. Volume 2. (2002) 140 ff.
15. Baker, S., Nayar, S.: Single viewpoint catadioptric cameras. In: PV01. (2001) 39–71
16. Svoboda, T., Pajdla, T.: Epipolar geometry for central catadioptric cameras. IJCV **49** (2002) 23–37
17. Swaminathan, R. Grossberg, M., Nayar, S.: Caustics of catadioptric cameras. In: ICCV02. (2001)
18. Fiala, M., Basu, A.: Panoramic stereo reconstruction using non-svp optics. In: ICPR02. Volume 4. (2002) 27–30
19. Yagi, Y., Kawato, S.: Panoramic scene analysis with conic projection. In: IROS90. (1990)
20. Yokoya, N., Iwasa, H., Yamazawa, K., Kawanishi, T., Takemura, H.: Generation of high-resolution stereo panoramic images by omnidirectional imaging sensor using hexagonal pyramidal mirrors. In: ICPR98. (1998)
21. Spacek, L.: Omnidirectional catadioptric vision sensor with conical mirrors. In: Towards Intelligent Mobile Robotics, TIMR03. (2003)
22. Lin, S., Bajcsy, R.: True single view point cone mirror omni-directional catadioptric system. In: ICCV01. Volume 2. (2001) 102–107
23. Hicks, A., Bajscy, R.: Reactive surfaces as computational sensors. In: The second IEEE Workshop on Perception for Mobile Agents. Held in Conjunction with CVPR'99. (1999) 82–86
24. Brassart, E., et al.: Experimental results got with the omnidirectional vision sensor: Syclop. In: EEE Workshop on Omnidirectional Vision (OMNIVIS'00). (2000) 145–152
25. Geyer, C., Daniilidis, K.: Structure and motion from uncalibrated catadioptric views. In: CVPR01. Volume 1. (2001) 279–286
26. Geyer, C., Daniilidis, K.: Paracatadioptric camera calibration. IEEE PAMI **24** (2002) 1–10
27. Lin, S., Bajcsy, R.: High resolution catadioptric omni-directional stereo sensor for robot vision. In: IEEE International Conference on Robotics and Automation, Taipei, Taiwan. (2003) 12–17
28. Spacek, L.: Edge detection and motion detection. Image and Vision Computing **4** (1986) 43–56
29. Sara, R.: Finding the largest unambiguous component of stereo matching. In: ECCV (3). (2002) 900–914